CrossMark

Electromagnetic modeling of periodically-structured fiber-reinforced single-layer laminate with multiple fibers missing

Z.-C. Liu[1] · **C.-Y. Li[2]** · **D. Lesselier[1]** · **Y. Zhong[3]**

Abstract Modeling of periodically-structured, fiber-reinforced laminates with fibers missing is investigated, this applying as well to similarly disorganized photonic crystals at optical frequencies. Parallel cylindrical fibers are periodically embedded within a layer sandwiched between two half-spaces. Absent fibers destroy the periodicity. The supercell concept involving an auxiliary periodic structure provides subsidiary solutions, wherein plane-wave illumination can be analyzed with the help of the Floquet theorem, while the field response due to a line source can be calculated from the pertinent plane-wave expansion. Accuracy, computational efficacy and versatility of the above approaches are illustrated by comprehensive numerical simulations with in particular comparisons to results provided by a finite-element code, all-purpose but computationally demanding, this work seen as the first step to the localization of missing fibers in a damaged laminate and imaging thereof.

1 Introduction

Fiber-reinforced composite laminates are increasingly used for their advantages in stiffness and strength in man-made parts in aeronautics, automotive industry and for green energy applications, while offering also interesting opportunities for shields and radomes, with no pretense to exhaustivity. In all such situations, ensuring reliable usage and proper fit to design constraints is necessary, and challenging issues of nondestructive testing and evaluation (NdT-NdE) are faced with.

Electromagnetic means are one testing/evaluation modality among a number (elastic, thermographic, X-ray), here from MHz to sub-THz operation frequencies depending upon electromagnetic and geometrical characteristics of the laminates. Also due to similarities of organization, methods developed for such composites can be directly extended to photonic crystals exhibiting a similar geometry, e.g., [1], and their behavior in case of disorganization is of interest as well. Yet, in all cases, to succeed, accurate forward models and fast simulation tools are needed, as exemplified already for fiber arrays assumed placed in air [2–4].

The laminates which one is concerned with herein, in still recognized restricted/simplifying fashion, consist of finitely thick planar layers overall sandwiched between two homogeneous isotropic half-spaces [5]. In each layer (matrix), longitudinally oriented circular cylindrical fibers of same cross section are periodically embedded, that being in principle up to infinity along the transverse direction, fiber orientations being expected to differ from one layer to the next.

A single-layer structure, as a fundamental brick of such a laminated structure, is focused onto in the present contribution, emphasis being on the modeling of the damaged case with multiple fibers missing.

With most analyses of wavefield scattering by periodic structures as in the aforementioned contributions and references therein including in particular [6], the field analysis can be concentrated onto the primary unit by applying the Floquet theorem from the field pseudo-periodicity.

✉ Z.-C. Liu
zicheng.liu@l2s.centralesupelec.fr

[1] Laboratoire des Signaux et Systèmes, UMR8506 (CNRS-CentraleSupélec-Univ. Paris Sud), Gif-sur-Yvette, France

[2] BioMedical-Electromagnetics Group, Engineering Product Department, Singapore University of Technology and Design, Singapore, Singapore

[3] A*STAR, Institute of High Performance Computing, Singapore, Singapore

However, since the periodicity is obviously destroyed due to absent fibers, this favorable prior knowledge becomes irrelevant.

Yet, the problem can still be tackled by introducing an auxiliary new periodic structure with each unit (supercell) [7, 8] including a limited number of fibers and the defects (here, those are the absent fibers) within the central area. Enlarging the transverse cell size and as a consequence the number of included elements (as said, both existing and absent fibers), the field computed inside, above and below (at least close enough to the laminate surface) the central region of the supercell is expected to converge to the true field, i.e., observed if the infinitely extended (damaged) laminate was effectively simulated, which is verified by numerical results here, given the lack of mathematical justification. Proper conditions of convergence should be met, depending upon operation frequencies, illuminations, material characteristics, and geometry.

The problem here is considered for plane wave and line source illuminations in E-polarized or Transverse-Electric (TE) and H-polarized or Transverse-Magnetic (TM) cases. Scattering of the field impinging onto the laminate from a line source is analyzed via a Fourier transform and numerical methods. The incident field is decomposed into plane-wave components with different amplitudes and incident angles. The total field is a superposition of the corresponding fields.

Detouring the integration path and shortening the integration interval are means further adopted to provide computation efficiency. Indeed, singularities of the integrand, associated to peculiar wavefield behaviors, emerge within a properly cut wavenumber complex plane, those possibly associated to peaks along the real line of integration and slow decrease along it when interested into very near fields. So, care is required here.

In Sect. 2, the plane-wave scattering is modeled. In Sect. 3, the line source case is detailed. In Sect. 4, numerical results are proposed. A brief conclusion follows, with insistence on imaging issues ahead.

2 Plane-wave illumination

The structure is sketched in Fig. 1. An infinite set of circular cylindrical fibers oriented along the y axis is embedded in an homogeneous planar slab bounded by upper and lower interfaces $z = a$ and $z = b$. Including the missing ones, fibers of radius c are periodically positioned along the x axis with period d. The space is then divided into Ω_{0+} and Ω_{0-} denoting half-spaces above and below, and Ω denoting the matrix containing the fibers, and Ω_l the fiber l.
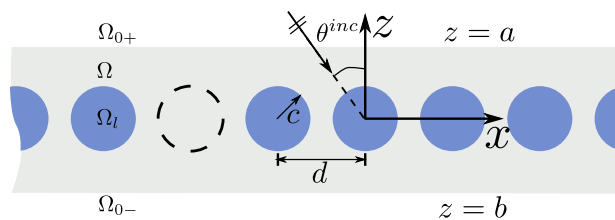

Fig. 1 Cross section of laminate with missing fiber

Time-harmonic dependence $\exp(-i\omega t)$, i imaginary unit, is implied. Materials are linear isotropic with relative dielectric permittivity (possibly complex-valued) and magnetic permeability ϵ_j, μ_j, $j = 0+, 0-, \cdot, l$, where $\cdot$ standing for null. Fibers are with $\epsilon_l = \epsilon_f$, $\mu_l = \mu_f$ except absent ones with $\epsilon_l = \epsilon$, $\mu_l = \mu$, subscript f holding for fiber material.

An unit-amplitude TM or TE plane wave obliquely illuminates the laminate with angle θ^{inc} and expression $V^{\text{inc}}(\mathbf{r}) = e^{i[\alpha_0 x - \beta_0(z-a)]}$, V as E_y or H_y field according to polarization, $\mathbf{r} = (x, z)$ the observation point, $\alpha_0 = k_{0+} \sin \theta^{\text{inc}}$, $\beta_0 = k_{0+} \cos \theta^{\text{inc}}$, k_{0+} the wavenumber.

The periodicity of the structure is destroyed by missing fibers, which forbids application of the Floquet theorem. An auxiliary periodic structure is then introduced. A "supercell", including multiple fibers (all those absent and a proper number of present ones), and repeated to infinity, is introduced as depicted in Fig. 2 with dashed separation lines, the analysis being carried out like with truly periodic structures.

Set the number of contained fibers (including missing ones) within the supercell to L. Based on the Floquet theorem, $V(x + sD, z) = V(x, z)e^{i\alpha_0 sD}$ [9], $D = Ld$, the field scattered by the l-th fiber in the s-th cell, $l = 1, 2, \ldots, L$, $s \in \mathbb{Z}$, can be multipole expanded as

$$V^{\text{sca}}_{l,s}(\mathbf{r}) = \sum_{m \in \mathbb{Z}} B^l_m g^{H^{(1)}}_m(x_l - sD, z_l)e^{i\alpha_0 sD}, \tag{1}$$

where $g^Z_m(x_l, z_l) = Z_m(kr_l)e^{im\theta_l}$, $Z = H^{(1)}$ denotes the first kind Hankel function, (x_l, z_l) are local coordinates of $\mathbf{r}$ w.r.t the coordinate system originating at the center of the l-th fiber, and $r_l = \sqrt{x_l^2 + z_l^2}$, $\theta_l = \arg(x_l + iz_l)$.
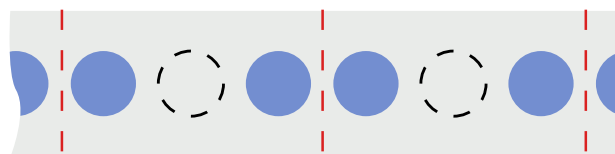
Then, the total scattered field is

Fig. 2 Sketch of the supercell structure, $L = 3$

$$V_{\text{tot}}^{\text{sca}}(\mathbf{r}) = \sum_{m\in\mathbb{Z}} \sum_{l=1}^{L} B_m^l \sum_{s\in\mathbb{Z}} g_m^{H^{(1)}}(x_l - sD, z_l) e^{isD\alpha_0}. \qquad (2)$$

To conveniently make use of the slab boundary conditions, $V_{\text{tot}}^{\text{sca}}(\mathbf{r})$ is transformed into plane-wave form. Letting $K_{m,p}^{\pm} = 2(-i)^m e^{\pm im\theta_p}/(D\beta_p)$, signs $+$ and $-$ corresponding to $z \geq 0$ and $z < 0$, $\alpha_p = \alpha_0 + 2\pi p/D$, $\beta_p = \sqrt{k^2 - \alpha_p^2} = k\sin\theta_p$, one has [10]

$$\sum_{s\in\mathbb{Z}} g_m^{H^{(1)}}(x_l - sD, z_l) e^{isD\alpha_0} = \sum_{p\in\mathbb{Z}} K_{m,p}^{\pm} e^{i\left(\alpha_p x_l \pm \beta_p z_l\right)}. \qquad (3)$$

The field in region Ω is the sum of $V_{\text{tot}}^{\text{sca}}$ and the field scattered by the slab boundaries, i.e., the field in Ω is

$$\begin{aligned} V(\mathbf{r}) = &\sum_{p\in\mathbb{Z}} \left[f_p^- e^{-i\beta_p z} + f_p^+ e^{i\beta_p z} \right] e^{i\alpha_p x} \\ &+ \sum_{p\in\mathbb{Z}} \sum_{m\in\mathbb{Z}} K_{m,p}^{\pm} F_m^p e^{i\left(\alpha_p x \pm \beta_p z\right)}, \end{aligned} \qquad (4)$$

wherein $F_m^p = \sum_{l=1}^{L} B_m^l e^{-i\alpha_p ld}$ is the discrete Fourier transform of B_m^l, and f_p^+/f_p^- are coefficients of the field scattered by the lower/upper slab boundary.

The total field above and below the slab reads as

$$V^{0+}(\mathbf{r}) = \sum_{p\in\mathbb{Z}} \left[\delta_{p0} e^{-i\beta_p^{0+}(z-a)} + r_p e^{i\beta_p^{0+}(z-a)} \right] e^{i\alpha_p x}, \qquad (5)$$

$$V^{0-}(\mathbf{r}) = \sum_{p\in\mathbb{Z}} t_p e^{-i\beta_p^{0-}(z-b)} e^{i\alpha_p x}; \qquad (6)$$

r_p and t_p represent the reflection and transmission coefficients for the p-th plane-wave component, and δ_{p0} is a Kronecker delta. With (4)–(6), matching the field at the slab boundaries yields r_p, t_p, f_p^+, f_p^- as function of F_m^p (or B_m^l).

To find B_m^l, one uses that the wave incoming upon the l-th fiber is made of fields scattered by all other fibers and the slab boundaries. Applying the Graf's addition theorem with the condition $r_l < d$, and Jacobi–Anger expansion, the field in the vicinity of the l-th fiber can be expanded into cylindrical functions as

$$V(\mathbf{r}) = \sum_{m\in\mathbb{Z}} \left[A_m^l J_m(kr_l) + B_m^l H_m^{(1)}(kr_l) \right] e^{im\theta_l}, \qquad (7)$$

where

$$A_m^l = \sum_{p\in\mathbb{Z}} e^{i\alpha_p ld} \left(J_{m,p}^+ f_p^+ + J_{m,p}^- f_p^- \right) + \sum_{j=1}^{L} \sum_{n\in\mathbb{Z}} S_{m,n}^{lj} B_n^j \qquad (8)$$

known as the Rayleigh identities; $S_{m,n}^{lj}$ is a relative lattice sum [7] weighting in the field contribution from the j-th fiber, $J_{m,p}^{\pm} = (i)^m \exp(\mp im\theta_p)$.

With the expressions f_p^+ and f_p^-, a linear relationship between A_m^l and B_m^l is established,

$$A_m^l = \sum_{j=1}^{L} \sum_{n\in\mathbb{Z}} \left(S_{m,n}^{l,j} + \Psi_{m,n}^{l,j} \right) B_n^j + K_m^l. \qquad (9)$$

Together with another one from the fiber boundary conditions, $B_m^l = R_m^l A_m^l$, B_m^l proceeds from

$$\mathbf{B} = (\mathbf{I} - \mathbf{R}\Theta)^{-1}(\mathbf{R}\mathbf{K} + \mathbf{T}\mathbf{Q}), \qquad (10)$$

with column vectors $\mathbf{A} = [A_m^l]$, $\mathbf{B} = [B_m^l]$, $\mathbf{K} = [K_m^l]$, $\mathbf{Q} = [Q_m^l]$ and matrices $\Theta = [S_{m,n}^{l,j} + \Psi_{m,n}^{l,j}]$, $\mathbf{R} = [R_m^l]$, $\mathbf{T} = [T_m^l]$.

3 Line source illumination

Set a line source at $\mathbf{r}_s$ in the upper half-space R_{0+}, the corresponding incident field being the Green function $H_0^{(1)}(k_{0+}|\mathbf{r} - \mathbf{r}_s|)/(4i)$, which can be expressed as [11]

$$V^s(\mathbf{r}, \mathbf{r}_s) = \frac{1}{4i\pi} \int_{-\infty}^{\infty} d\alpha_0 \frac{e^{i\alpha_0 x + i\beta_{0+}|z|}}{\beta_{0+}}, \qquad (11)$$

in which the integrand indicates a plane wave as function of α_0. Taking $e^{i(\alpha_0 x - \beta_{0+} z)}/\beta_{0+}$ as incident waves, with the modeling approach of Sect. 2, the scattered field denoted as $V(\alpha_0)$ can be readily obtained. Then, the total field due to the line source is

$$V(\mathbf{r}, \mathbf{r}_s) = \frac{1}{4i\pi} \int_{-\infty}^{\infty} d\alpha_0 V(\alpha_0), \qquad (12)$$

which can be dealt with by numerical methods.

However, branch points and poles in $V(\alpha_0)$, may complicate the integration and consequently slow down the convergence sought. Two techniques are adopted to alleviate the above, detouring the integration path and reducing the integration interval. Singularities are periodic with period $2\pi/D$ [12], and thus the detoured path is defined as $\alpha_0^* = \alpha_0 - i\gamma\sin(D\alpha_0)$, γ amplitude of the imaginary part, as shown in Fig. 3. The complex plane of α_0^* is defined in the top Riemann sheet ($\Im(\beta_j) > 0$). Singularity points are surrounded and the convergent rate benefits from the
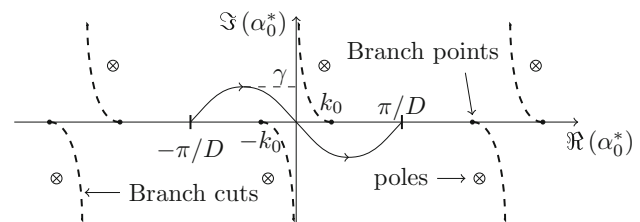

Fig. 3 Sketch of branch cuts/points, poles and detoured path in complex α_0^* plane when $k_{0+} = k_{0-}$

smoother integrand. The other acceleration comes from the rewritten form of (11),

$$V^s(\mathbf{r}, \mathbf{r}_s) = \frac{1}{4i\pi} \sum_{p \in \mathbb{Z}} \int_{-\pi/D + p\frac{2\pi}{D}}^{\pi/D + p\frac{2\pi}{D}} d\alpha_0 \frac{e^{i\alpha_0 x + i\beta_{0+}|z|}}{\beta_{0+}}$$
$$= \frac{1}{4i\pi} \int_{-\pi/D}^{\pi/D} d\alpha_0 \sum_{p \in \mathbb{Z}} \frac{e^{i\alpha_p x + i\beta_p^{0+}|z|}}{\beta_p^{0+}} .$$

(13)

Replacing δ_{p0} in (5) by $1/\beta_p^{0+}$, multiple sampling points of α_0 can be computed in a single calculation without additional cost, and the integration interval is reduced from $[-\infty, \infty]$ to $[-\pi/D, \pi/D]$.

4 Numerical illustrations

Focus is on a single-layer laminate sandwiched by air containing graphite fibers ($\epsilon_f = 12$, conductivity $\sigma = 330$ S/m), with limiting value of perfect electric conductivity (PEC), and glass fibers ($\epsilon_f = 6$, negligible losses). Matrix is always epoxy ($\epsilon = 3.6$, loss tangent 0.02). Slab boundaries are at $a = -b = d/2$, $d = 0.1$ mm. These parameters could be adjusted as needed. L is taken odd so as fibers in the primary cell are indexed from $-(L-1)/2$ to $(L-1)/2$. Both well-organized and disorganized laminates are considered, the latter signaled by χ as set of indices of missing fibers. The global coordinate system originates at the 0-th fiber center.

Infinite series $\sum_{m \in \mathbb{Z}}$ and $\sum_{p \in \mathbb{Z}}$ are truncated as $\sum_{m=-M}^{M}$ and $\sum_{p=-P}^{P}$. P and M should be such that enough evanescent waves or high-order multipole components are included in the expansion. When $r_l < d$, the field outside the l-th fiber can be computed by plane-wave expansion (4) or multipole expansion (7). With a well-organized structure, Fig. 4 shows the values of $|V_p - V_m|$ versus P and M, V_p, V_m as field intensity at $(0, 0.4d)$ via plane-wave and

multipole expansion, resp. With $M = 17, P = 30$, $|V_p - V_m|$ is less than 10^{-6}. For general cases, high accuracy is guaranteed with formulas $M = \text{Int}(\Re(4.05 \times (kc)^{1/3} + kc))$, $P = \text{Int}(D(3\Re(k) - \alpha_0)/2\pi)$ [9].

To further validate supercell modeling, comparisons with results from the finite-element COMSOL software are performed by configuring the two sides of the slab with periodic condition. Define reflection and transmission coefficients as $R_p = \Re\left(\left(\beta_p^{0+}\right)^* r_p r_p^* / \beta_0^{0+}\right)$, $T_p = \Re\left(\left(\beta_p^{0-}\right)^* t_p t_p^* / \beta_0^{0+}\right)$ [13], $*$ denoting conjugation. With $\chi = [-1, 1]$, Fig. 5a, b show comparisons of R_0 with
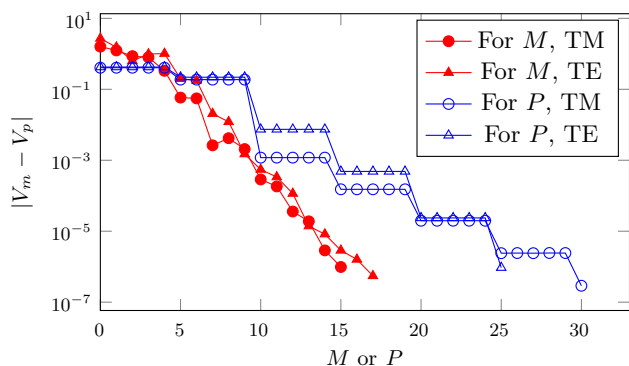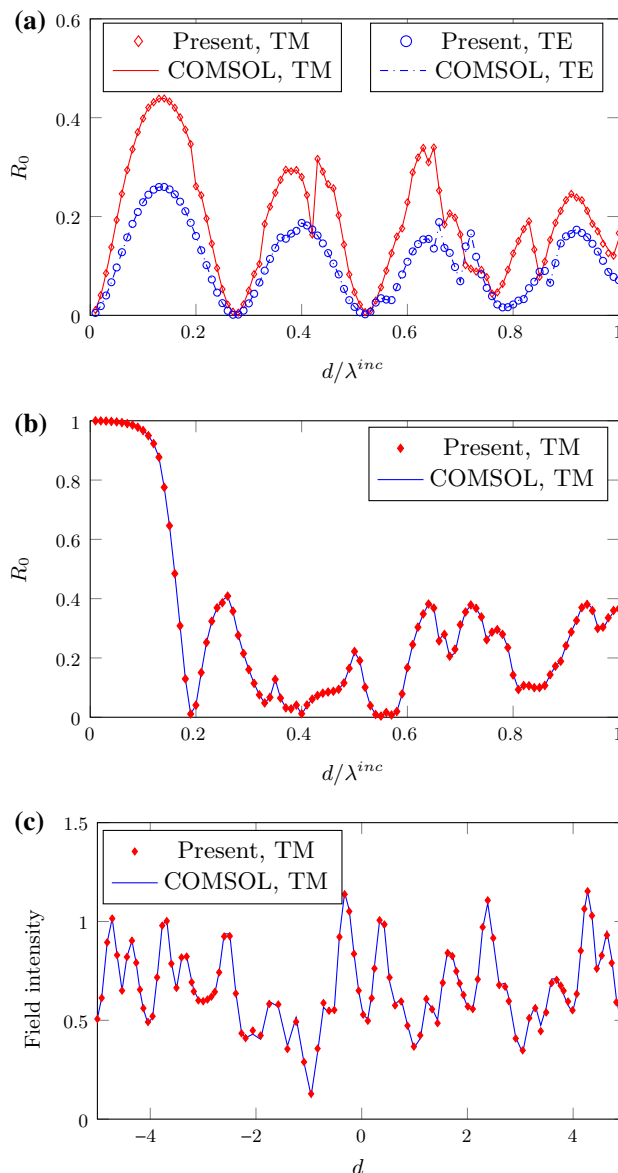

Fig. 4 Convergence of field expansion versus P and M for well-organized glass-fiber laminate, $\lambda^{inc} = d = 0.1$ mm, $c = 0.25d$, $L = 5$

Fig. 5 Comparisons of R_0 in (a) and (b) with $\theta^{inc} = \pi/6$, $c = 0.25d$, $L = 5$, $\chi = [-1, 1]$, and field intensities in (c) with $\lambda^{inc} = d$, $c = 0.4d$, $L = 31$, $\chi = [-2, -1, 1, 3]$
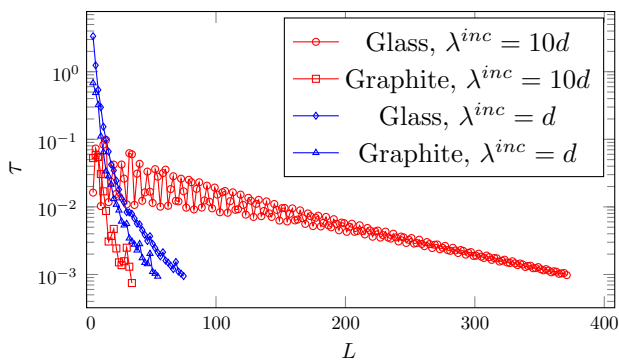
Fig. 6 Relative convergence versus L with plane-wave illumination of two types of disorganized laminate, $\theta^{\text{inc}} = 0$, $c = 0.2d$, $\chi = [-1, 1]$

Fig. 7 Number of samples in QUADCC with various γ for line source above a well-organized graphite-fiber laminate, $\mathbf{r}_s = (0, a + d)$, $c = 0.25d$, $\lambda^{\text{inc}} = 10d$

Fig. 8 Comparisons of fields in TM case, $\mathbf{r}_s = (0, a + d)$, $c = 0.25d$, $\chi = [-1, 1]$ and $L = 81$ for the disorganized laminate, denoted by "Dis", while "Well" is for well-organized. **a** Graphite fiber, $\lambda^{\text{inc}} = 10d$. **b** Glass fiber, $\lambda^{\text{inc}} = d$

different wavelengths with glass or PEC fibers, for plane-wave illumination. To validate all R_p (including evanescent field components), comparisons of the fields sampled along the line $-5d \leq x \leq 5d$, $z = 0.45d$ are depicted in Fig. 5c with graphite fibers of radius enlarged to $0.4d$ and $\chi = [-2, -1, 1, 3]$.

The COMSOL mesh size should be small enough for accuracy that being paid by high computational cost. With configurations as in Fig. 5c, the proposed approach costs 1.2s and COMSOL $\approx$ 30 times more for the same laptop which has dual cores with clock speeds 2.9 GHz.

Fields in the central area of the supercell show convergence with increasing L. With 100 equally spaced points along the line $z = 2d$, $-5d \leq x \leq 5d$, denoting ϕ_k^j as the data collected at the j-th point for $L = 2k + 1$, the relative convergence error is defined as $\tau_L = \max_j \left| \phi_{k+1}^j - \phi_k^j \right| / \left| \phi_{k+1}^j \right|$. With $\chi = [-1, 1]$, values of τ_L are shown in Fig. 6. The line graphs stop when τ_L is below 10^{-3}. With lossless glass fibers, the larger wavelength leads to a smaller imaginary part of the epoxy wavenumber and poor field convergence [8].

In modeling line sources, γ (the amplitude of the imaginary part of the defined detouring path) affects the computation efficiency. The recently introduced package QUADCC [14], which in particular obeys Clenshaw–Curtis quadrature rules, is adopted to perform the integration. Testing with intact structure, Fig. 7 shows the number of required samples with different γ. When $\gamma = 10$ and $\gamma = 100$, the sampling number is indeed smaller than by integrating along the real axis ($\gamma = 0$). However, too large a γ may slow down the convergent rate. In time cost, it is 1200s for point $(0, 0.5c)$ with $\gamma = 0$, $\approx 60\%$ with $\gamma = 100$ and $\approx 130\%$ with $\gamma = 1000$.

Validations for line source illumination are performed by comparing fields along the line $z = 0.5c$, $-5d \leq x \leq 5d$. Both COMSOL and the supercell approach are run with 81 fibers, save that the periodic condition is not configured anymore in COMSOL, so that it should return the solution
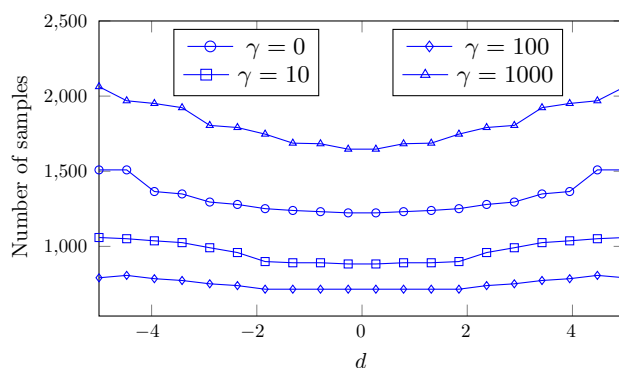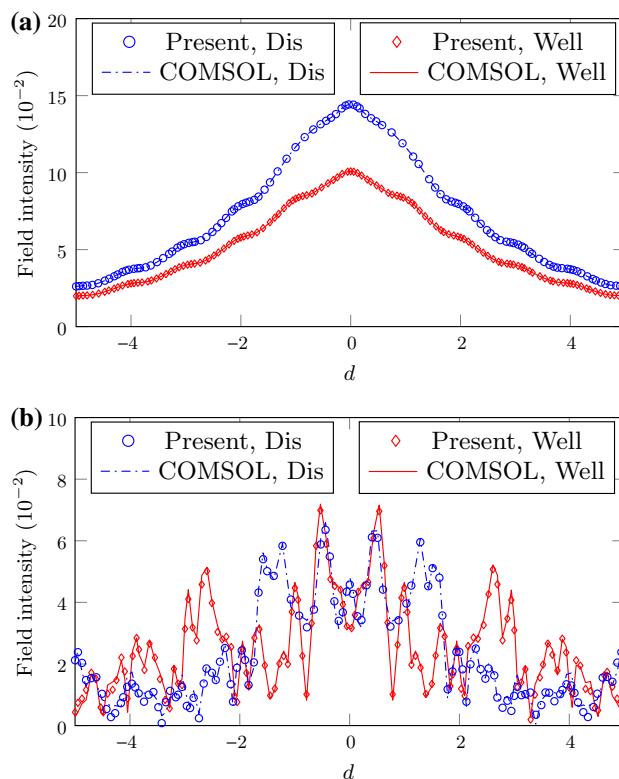
for the true laminate. As shown in Fig. 8a, b, with glass or graphite fiber, results for a well-organized and a disorganized structure ($\chi = [-1, 1]$) fit well.

Accuracy of the modeling is also checked by testing reciprocity. The line source above an intact structure is at $(0, a + 2d)$ and observing the field along the line $-5d \leq x \leq 5d$, $z = a + d$, with V_1 as collected data vector. Exchanging source and observer positions yields V_2.
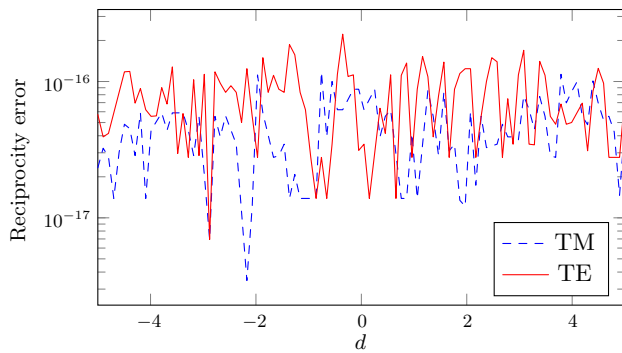
Fig. 9 Reciprocity error versus sampling, graphite-fiber disorganized laminate, $\lambda^{\text{inc}} = 10d, c = 0.25d, \chi = [-1, 1]$

Values of $|V_1 - V_2|$ are drawn as the line graph in Fig. 9, with amplitude $\sim 10^{-16}$.

5 Conclusion

By means of an auxiliary supercell periodic structure, fiber-reinforced laminates and alike structures with defects as missing fibers can be successfully dealt with, illuminations by plane waves and line sources in the TM and TE polarization cases being proposed herein. Decomposing a line illumination into plane waves, the field indeed is a superposition of scattered fields by plane-wave elements, which can be computed by fast numerical methods as analyzed.

The results are validated by a general-purpose finite-element software, and modeling accuracy and convergence of the field are exhibited.

The work focused onto the case of fibers missing. Fiber displacement and shrinkage and bubbles inside and outside a fiber can be investigated likewise.

Yet, the main step ahead is to image defects of the laminates, in the presently described situation, missing fibers. Various imaging algorithms, such as MUSIC [15] and sparsity-dedicated approaches [16], are being contemplated to that effect, preliminary results being available from [17] from multi-static multi-frequency data in reflection mode.

Other pending issues involve enhancement of resolution via (if accurate enough by the present approach) homogenization of a sound laminate [18] since at wavelength large enough versus the diameter of fibers an equivalent medium can be reached, and closed-form Green functions in TE and TM cases follow (with complex behaviors in the spectral domain), missing fibers then being just small defects that can be modeled according to first-order approximations and imaged in harmony.

Also, this a priori tailored to photonic structures and not to laminates of the industry as currently tested, resonating

structures could be modeled, potentially leading to super-resolved imaging [19].

References

1. C.Y. Li et al., Recursive matrix schemes for composite laminates under plane-wave and Gaussian beam illumination. J. Opt. Soc. Am. B. **32**, 1539–1549 (2015)
2. J.-P. Groby, D. Lesselier, Localization and characterization of simple defects in finite-sized photonic crystals. J. Opt. Soc. Am. A **25**, 146–152 (2008)
3. K. Watanabe et al., Accurate analysis of electromagnetic scattering from periodic circular cylinder array with defects. Opt. Express **20**, 10646 (2012)
4. Z.C. Liu et al., Electromagnetic modeling of a periodic array of fibers embedded in a panel with single fiber missing, in *Electromagnetic Non-destructive Evaluation*, vol. XIX, ed. by N. Yusa, et al. (IOS Press, Amsterdam, 2016), pp. 237–244
5. C.Y. Li et al., Full-wave computational model of electromagnetic scattering by arbitrarily-rotated 1-D periodic multilayer structure. IEEE Trans. Antennas Propagat. **64**, 1047–1060 (2016)
6. J.-P. Groby et al., Acoustic response of a rigid-frame porous medium plate with a periodic set of inclusions. J. Acoust. Soc. Am. **126**, 685–693 (2009)
7. L.C. Botten et al., Formulation for electromagnetic scattering and propagation through grating stacks of metallic and dielectric cylinders for photonic crystal calculations. Part I. Method. J. Opt. Soc. Am. A **126**, 2165–2176 (2000)
8. M.D. Sterke et al., Defect modes in otherwise perfect photonic crystals and photonic crystal fibers. Proc. SPIE (2005). doi:10.1117/12.620657
9. C.Y. Li et al., Electromagnetic small-scale modeling of composite panels involving periodic arrays of circular fibers. Appl. Phys. A **117**, 567–572 (2014)
10. K. Watanabe, Y. Nakatake, Spectral-domain formulation of electromagnetic scattering from circular cylinders located near periodic cylinder array. PIER B **31**, 219–237 (2011)
11. W.C. Chew, *Waves and Fields in Inhomogeneous Media* (IEEE Press, New York, 1995)
12. F. Capolino et al., Fundamental properties of the field at the interface between air and a periodic artificial material excited by a line source. IEEE Trans. Antennas Propagat. **53**, 91–99 (2005)
13. J.A. Kong, *Electromagnetic Wave Theory* (EMW, Cambridge, 2008)
14. P. Gonnet, Increasing the reliability of adaptive quadrature using explicit interpolants. ACM TOMS **37** (2010)
15. R. Schmidt, Multiple emitter location and signal parameter estimation. IEEE Trans. Antennas Propagat. **34**, 276–280 (1986)
16. O.K. Lee et al., A non-iterative method for the electrical impedance tomography based on joint sparse recovery. Inverse Probl. **31**, 075002 (2015)
17. Z.C. Liu et al., Electromagnetic retrieval of missing fibers in periodic fibered laminates via sparsity concepts, in *Proceedings of the 2016 European Signal Processes Conference*, (EUSIPCO), Budapest, IEEE CFP1640S-USB, pp. 345–349 (2016)
18. H. Ammari et al., Enhanced resolution in structured media. SIAM J. Appl. Math. **70**, 1428–1452 (2009)
19. H. Ammari, H. Zhang, A mathematical theory of super-resolution by using a system of sub-wavelength Helmholtz resonators. Commun. Math. Phys. **337**, 379–428 (2015)